Modeling Atmospheric Chemistry and Transport with Dynamic Adaptive Resolution

Emil M. Constantinescu (emconsta@cs.vt.edu) and Adrian Sandu (asandu@cs.vt.edu)
Department of Computer Science, Virginia Polytechnic Institute and State University, Blacksburg, VA 24061.

Gregory R. Carmichael (gcarmich@cgrer.uiowa.edu)
Center for Global and Regional Environmental Research University of Iowa; 204 IATL, Iowa City, IA

May 3, 2007

Abstract. We discuss an adaptive resolution system for modeling regional air pollution based on the chemical transport model STEM. The grid adaptivity is implemented using the generic adaptive mesh refinement tool Paramesh, which enables the grid management operations while harnessing the power of parallel computers. The computational algorithm is based on a decomposition of the domain, with the solution in different subdomains being computed with different spatial resolutions. Various refinement criteria which adaptively control the fine grid placement are analyzed in order to maximize the solution accuracy while maintaining an acceptable computational cost. Numerical experiments in a large scale parallel setting (~0.5 billions variables) confirm that adaptive resolution, based on a well chosen refinement criterion, leads to the decrease in spatial error with an acceptable increase in computational time. Fully dynamic grid adaptivity for air quality models is relatively new. We extend previous work on chemical and transport modeling by using dynamically adaptive grid resolution. Advantages and shortcomings of the present approach are also discussed.

Keywords: air pollution modeling; adaptive mesh refinement; chemical and transport models

"The original publication is available at www.springerlink.com."
(Published in Computational Geosciences; DOI: 10.1007/s10596-007-9065-7)

1. Introduction

The chemical composition of the atmosphere is being significantly perturbed by anthropogenic emissions of trace gases and aerosols. Air pollution has important implications for urban and regional air quality, for human health, and for climate change. Comprehensive atmospheric chemical and transport models (CTMs) are used to study the fate of atmospheric chemical constituents associated with the gas and aerosol phases.

Inadequate grid resolution can be an important source of errors in CTMs. In air pollution simulations large spatial gradients of tracer concentrations result from the complex interactions between emissions, meteorological conditions, and nonlinear atmospheric chemistry (Srivastava et al., 2001b; Srivastava et al., 2001a). Coarse grids artificially diffuse these large gradients, which in the presence of highly non-linear chemistry may affect considerably the predicted levels of pollutant concentrations.

Chock et al. (2002) studied the effects of grid resolution on model predictions of non-homogeneous atmospheric chemistry. They considered three different grid sizes, fine, medium and coarse. They concluded that coarse resolution leads to a reduction of the suppression of ozone (O_3) in the presence of high nitrogen oxides (NO_x), and a reduction in the effectiveness of the NO_x inhibition effect. In one of their scenarios, the nitrogen monoxide (NO) peak concentration decreases by 76% as the grid size increases from fine to coarse. Ozone loses nearly all the detail near the emission source in the coarse grid case.

A popular multi-resolution approach in air quality and meteorological modeling is static nesting of finer grids into coarser grids (Park et al., 2004; Wang et al., 2004). This approach requires apriori knowledge of where to place the high resolution sub-grids inside the modeling domain; however, it does not adjust to dynamic changes in the solution during simulation. In many practical situations, the modeler "knows" where higher resolution is needed, for example above industrial areas. However, changing meteorological fields (e.g., wind velocity) may prompt unsteady fine grid placement. Furthermore, there are situations in which sporadic events like biomass burning require dynamic resolution adjustment (Unal and Odman, 2003).

In this paper we present an application of adaptive mesh refinement (AMR) to model regional air quality. The grid adapts dynamically during the simulation, changing the grid resolution at certain intervals (regriding frequency), with the purpose of controlling the numerical spatial discretization error. Adaptive refinement is (1) more computationally efficient than uniform refinement and (2) more flexible than static grid nesting, since with AMR the user does not have to specify in advance which areas need higher resolution; instead, a refinement criterion is defined and then used by the code to automatically adjust the grid.

In this study we use the generic AMR tool Paramesh (MacNeice and Olson, 2003) that allows to harness the power of parallel computers for regional air pollution simulations. Parallel computing is needed since, the higher the resolution, the more expensive the simulation becomes. In addition, there is overhead associated with the management of the

non-uniform grid and with interpolating the solution between different grid levels. The generic tools allow different models to benefit from the AMR techniques without the huge overhead of implementing the grid management system. Moreover, the air quality model can benefit from subsequent improvements in the grid management system.

Atmospheric chemical and transport modeling in the AMR framework raises a number of challenging questions regarding the error control that defines the refinement criterion. In terms of effectiveness, the issues are which species should be considered for refinement and where to place the fine grids in order to obtain an accurate solution. In terms of efficiency, the questions are how often should the regriding operation take place and how much should one refine to gain a good accuracy–workload trade-off.

In this work we focus on the ozone concentration field. We extend the previous work on chemical and transport systems using an adaptive resolution and propose new research avenues. The main contributions of this paper are the following: We show that (I) high resolution grids need to be placed not only above sources, but also upwind of the regions of interest; (II) the refinement criterion should be based both on the species of interest and on their chemical precursors. Furthermore, in this work (III) we propose different refinement criteria, (IV) investigate the regriding frequency for maximum efficiency, and (V) analyze parallelization approaches. The last contribution points to a large body of future research in high performance computing related to large scale simulations.

The paper is organized as follows. Section 2 gives an overview of previous work. A brief description of the static fixed mesh air pollution modeling application used in this paper is given in Section 3. The approach taken for adaptive mesh refinement is explained in Section 4. Numerical results are shown in Section 5, and Section 6 presents conclusions and future research directions.

2. Previous Work

Adaptive meshes have been used in the study of pollutant dispersion in both atmosphere (Boylan et al., 2002; van Loon, 1996; Srivastava et al., 2001b; Srivastava et al., 2001a; Odman and Russell, 1991; Odman et al., 2002; Ghorai et al., 2000; SAIC, 2003) and water (Borthwick et al., 1998). In this section we discuss several atmospheric AMR applications.

The Ph.D. dissertation of van Loon (1996) is focused on numerical methods for smog prediction. The model developed, CWIROS, has 4 vertical layers and its horizontal domain covers all Europe. The

author proposes a two dimensional structured AMR technique in the horizontal direction (named local uniform grid refinement). In CWIROS applications, the base grid horizontal resolution is about 60×60 Km with 4 levels of refinement and a fine grid resolution of about 7.5×7.5 Km. The spatial error estimator uses the curvature of the concentration fields and takes into account different species and layers with an appropriate weight. The curvature is scaled by the maximum value of each component in the corresponding layer. The column is flagged for refinement if the error estimator is larger than a user prescribed tolerance. Van Loon concludes that only advection and emission processes can generate or move sharp spatial gradients, and only these two processes should be looked at for dynamically adjusting the grid. Consequently, regriding is done at each advection step. The solution is advanced in time at all grid levels. Numerical experiments indicate that in some instances grid refinement leads to a better agreement between the model and observations; while in other instances, the agreement is not improved significantly.

Srivastava et al. (2001b) discuss a very interesting approach to grid adaptivity (DSAGA-PPM) for simulating reactive atmospheric pollutants. DSAGA-PPM uses horizontal (2D) adaptivity and employs a constant number of grid nodes. This keeps the total computational time for a simulation manageable. The solution procedure is based on cell-centered finite volume procedures for advancing the solution on a nonuniform structured grid. A weight function is defined by a linear combination of curvatures of different chemical species. Based on this weight function the grid is adapted, i.e., the nodes are repartitioned such that they are clustered in areas of high weight, where more resolution is needed. Next, the meteorological and emission fields are remapped onto the new grid locations, and the concentration fields are obtained on the new grid via solving an additional advection equation related to the movement of the grid. This procedure is repeated iteratively since the rearrangement of tracer mass changes the weight function, which may require further adaptation of the grid. Once all the data are mapped onto the new grid, a finite volume method (within operator splitting approach) is used to advance the solutions to the new time level.

Odman et al. (2002) use their adaptive grid approach to simulate ozone air quality in the Tennessee Valley region for the July 7-17, 1995 period. Meteorological data are mapped onto the refined grids from a very high resolution mesoscale model simulation. The air pollution model accounts for more than 9000 point sources in the domain. The curvature of the surface layer NO concentrations provides the criterion for adjusting the grid resolution. The initial grid has a 8×8 Km initial

resolution, which is reduced to a few hundred meters around large point sources. Consequently the overall time step drops to less than one minute for maintaining a constant Courant number, which makes the simulation less efficient. The authors used time-splitting methods to circumvent this problem in a later study (Odman and Hu, 2007). The simulated NO and O_3 fields show a high level of detail. Similar conclusions are obtained by Boylan et al. (2002). They use a similar approach with static adaptive grids to model pollutants over Eastern US. Other refinement criteria have been investigated by M.N. Khan (Khan, 2003), including a a sensitivity based approach to determine the weights.

Ghorai et al. (2000) apply fully three-dimensional adaptive grid techniques to atmospheric dispersion problems. Their solution procedure uses a finite volume cell vertex approach on unstructured grids (tetrahedral elements). The adaptation procedure is based on refining and derefining element edges based on the values of mean solution and gradient along the specific edge. Edges that are cutting through large solution gradients are refined more. The authors present several experiments of pollutant dispersion from a single source in stable, neutral, and unstable boundary layers. They establish that the fully adaptive grid is able to represent the structures of a plume much more accurately than a statically nested grid with high resolution near the source. Also, their results show that adapting the vertical grid resolution dynamically results in a better resolution of the boundary layer plume values.

3. Regional Air Pollution Modeling

The core science application used in this paper is the state–of–the–art regional air quality model, Sulfur Transport Eulerian Model (STEM), (Carmichael, 2003; Carmichael et al., 2003). The original code uses a fixed grid, with all the data structures being multidimensional arrays to solve the mass-balance equations for concentrations of trace species in order to determine the fate of pollutants in the atmosphere (Sandu et al., 2005).

In STEM, the evolution of N_{spec} species is described by the following equations

$$\begin{aligned}
\frac{\partial c_s}{\partial t} &= -u\nabla c_s + \frac{1}{\rho}\nabla(\rho K \nabla c_s) + \frac{1}{\rho} f_s(\rho c) + E_s,\ t^0 \le t \le t^F,\ 1 \le s \le N_{\text{spec}}, \\
c_s(t^0, x) &= c_s^0(x), \\
c_s(t, x) &= c_s^{\text{in}}(t, x) \quad \text{for} \quad x \in \Gamma^{\text{in}},
\end{aligned} \tag{1}$$

$$K\frac{\partial c_s}{\partial n} = 0 \quad \text{for} \quad x \in \Gamma^{\text{out}},$$
$$K\frac{\partial c_s}{\partial n} = V_s^{dep} c_s - q_s \quad \text{for} \quad x \in \Gamma^{\text{ground}},$$

on a 3-D domain, where the concentration c_s for species s is dictated by q_s, the rate of surface emissions, E_s the rate of elevated emissions, and f_s, the rate of chemical transformation for this species. Further, u denotes the wind field vector, K the turbulent diffusivity tensor, ρ the air density, c^{in} the Dirichlet boundary conditions, and V_s^{dep} the deposition velocity. The boundaries $\Gamma^{\{\text{in,out,ground}\}}$ represent the inflow, outflow, and ground boundaries, respectively.

The equation is solved using an operator splitting approach. STEM uses linear finite difference discretization of the transport terms. Horizontal transport is solved using a directional x and y split approach with the third order one-dimensional upwind finite difference formula (Sandu et al., 2005). The diffusion terms are discretized using second order central differences. The advection inflow boundary uses a first order upwind scheme, which makes the order of entire scheme quadratic for the interior points. The vertical advection scheme is discretized by first order upwind finite difference and the diffusion term is discretized by the second order central scheme (Sandu et al., 2005). Atmospheric chemical kinetics results in stiff ODE equations that use a stable numerical integration that preserve linear invariants. The gas phase mechanism is SAPRC-99 (Carter, 2000) which considers 235 atmospheric reactions of volatile organic (VOCs) and nitrogen oxides (NO_x), in total of 93 species (88 variable and 5 constant), in urban and regional settings. The chemistry time integration is done by Ros-2 numerical integrator (Verwer et al., 1999), automatically generated by the software package KPP (Sandu et al., 2005; Damian et al., 2002).

4. The Adaptive Mesh Refinement Approach

Paramesh (MacNeice and Olson, 2003; MacNeice et al., 2000; Olson and MacNeice, 2005; Olson, 2006) is a parallel adaptive mesh refinement FORTRAN toolkit developed by P. MacNeice and K. Olson at the NASA Goddard Space Flight Center. Paramesh offers an infrastructure for adaptive mesh refinement on a 2D structured grid.

The adaptive resolution is based on a Schwarz-type domain decomposition, with a single Schwarz iteration: The domain is divided into blocks, with each block containing NXB × NYB cells plus several levels of guard-cells along each boundary, as shown in Figure 1.a.

Before advancing the solution in time, the guard-cells of each block are filled with values based on the values of the neighboring blocks or domain boundary. This involves copy operations (of solution values) if the two neighbors have the same refinement level, or an interpolation if the two neighbors have different refinement levels. With the guard-cells filled, the solution is computed independently in each block. Note that multiple iterations could be performed: The new solution is used to fill in the guard-cells, and with these updated boundary values the block solution could be computed again.

Paramesh provides the possibility of refining and derefining parts of the grid as we describe in the next section. The block entities are self similar with fixed orientation, and thus, the same numerical methods can be applied on all blocks regardless of their position or refinement level. Paramesh manages data migration (from processor to processor) in order to maintain their relative locality (i.e., "neighboring" data are assigned on the same processor) and processor load balancing.

4.1. G S

We use a two-dimensional (horizontal) grid refinement approach. All the data within a column in the original STEM data structures (i.e., data associated with the same projected longitude and latitude and all altitude levels) are assigned to a mesh point (cell) in Paramesh, including geographical and meteorological data, and species concentrations.

The choice of having a 2D mesh instead of a 3D one is partly imposed by the vertical data dependency given in the radiation code. The solar radiation code provides photolysis reaction coefficients which are calculated top-bottom for each column. The dependency is due to the fact that each layer may absorb or reflect a variable amount of energy from the radiation spectrum. This is due to several factors: the species concentration (e.g., O_3, carbon monoxide (CO)), dust, cloud presence, or atmospheric water content. A full 3D approach leads to more complicated data dependencies and more communication among grid-cells situated on the same column yielding an all-to-all data dependency within each column. This approach can, potentially, make the parallel application almost sequential due to the radiation calculation which is in itself computationally expensive.

The domain is divided into blocks, each block contains 6×6 cells plus two guard-cells along each boundary (see Fig. 1.a). At the coarse level, each cell has a resolution of 80×80 Km and therefore each block covers 480×480 Km. For the TraceP test simulation over East Asia (described in Section 5.1), the computational domain is covered by 15×10 blocks; i.e., 90×60 cells. At the finest level (level 4) each cell has

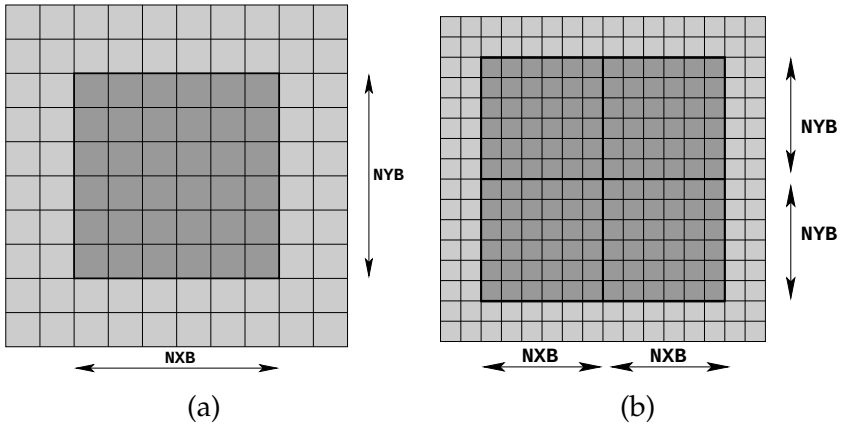

Figure 1. Paramesh block representation. (a) A block with NXB × NYB cells with two levels of guard-cells. In (b) the same block refined with an extra level.

a resolution of 10×10 Km. Refining and derefining consist in dividing or merging blocks until the coarsest or finest level are reached. In two dimensions, a refined block is split into four blocks each with the same number of cells and thus, each refined cell at level k+1 covers one fourth of the surface occupied by a cell at level k (see Figure 1.b). The derefining operation merges four blocks into one coarser block.

Data on each point are linearly interpolated during each mesh refinement-derefinement operation. The criteria for block refinement and derefinement are explained the next section.

4.2. T R D C

The estimation of the spatial error in a NXB × NYB horizontal block (at vertical level k) is done using the horizontal curvature of the concentration field c at each point (i, j, k) in space. This criterion is very popular in the literature (Odman and McRae, 2003). The curvature error estimation is given at each node by

$$err_{i,j,k} = \left| c_{i+1,j,k} - 2c_{i,j,k} + c_{i-1,j,k} \right| + \left| c_{i,j+1,k} - 2c_{i,j,k} + c_{i,j-1,k} \right| ,$$

and by taking the root mean square value normalized by the maximum concentration inside the block

$$ERR_k(c) = \begin{cases} \dfrac{\sqrt{\dfrac{1}{\mathrm{NXB} \times \mathrm{NYB}} \displaystyle\sum_{i,j} err_{i,j,k}^2}}{\max\limits_{i,j} c_{i,j,k}} & \text{if } \max\limits_{i,j} c_{i,j,k} \geq Atol \\ 0 & \text{if } \max\limits_{i,j} c_{i,j,k} < Atol \end{cases} .$$

Note that the error is ignored if the concentration itself inside the block is small enough, below a user-prescribed level of significance. For each horizontal layer we have one such error estimate, and the total estimate in the column is taken to be the maximum among all layers

$$ERR(c) = \max_k \; ERR_k(c)\,.$$

The block is flagged for refinement if

$$ERR(c) \geq uptol$$

and is flagged for derefinement if

$$ERR(c) \leq lowtol\,.$$

Another approaches of estimating the local errors can be based on the gradient magnitude

$$err_{i,j,k} \;\approx\; \left|c_{i+1,j,k} - c_{i-1,j,k}\right| + \left|c_{i,j+1,k} - c_{i,j-1,k}\right|\,.$$

Other approaches can be based on the effective or analytical truncation errors. The effective error estimation quantifies the error by using the difference between the current discretization method and an inexpensive lower order method. The analytical truncation error can be approximated from the magnitude of leading error term (i.e., coefficient of the first error term in the Taylor series expansion) of the current discretization method employed by the application. In this work we only focus on the field curvature to approximate the errors.

The model calculates the concentrations of a large number of pollutants, and the refinement pattern depends on which concentrations are used for error estimation. We consider both single and multiple chemical species criteria, and we focus on O_3 and some of its main chemical precursors: formaldehyde (HCHO) and NO_x (= NO and NO_2) compounds. The chemical species or their combination under consideration are: O_3, NO_x, and M, where M = NO_x and O_3 and HCHO. For the multiple species criterion based on ℓ chemical species, $i = 1, \cdots, \ell$, the error is estimated using a weighted linear combination:

$$ERR(c_1 \ldots c_\ell) = \sqrt{\frac{1}{\ell}\sum_{j=1}^{\ell} w_j\, ERR(c_j)^2}\,,$$

where w_j is the weight associated with the chemical species c_j. For instance, for the M criterion we consider the above mentioned chemical

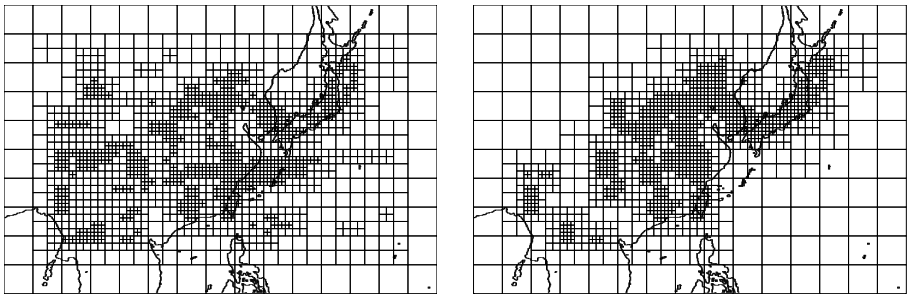

(a) M criterion (b) NO_x criterion

Figure 2. The refined grids at 0 GMT of March 1st, 2001 for East Asia during the TraceP campaign. Each block (shown) consists of 6×6 computational cells (not shown). The criterion is the curvature of (a) M and (b) NO_x, with $uptol = 0.25$ and $lowtol = 0.1$ and with maximum refinement level of 4 (10×10 Km). In general these criteria refine the areas of high emissions, i.e., above industrial regions in China, Japan, and Korea.

species: w_1NO + w_2NO$_2$ + w_3O$_3$ + w_4HCHO, with $w_1 = w_2 = 35\%$ and $w_3 = w_4 = 15\%$, and for NO_x criterion we take $w_1 = w_2 = 50\%$ and $w_3 = w_4 = 0\%$.

Next, we show some sample grids as they get refined according to two of our criteria. In the experiments below we used $uptol = 0.25$ and $lowtol = 0.1$. The refined grid patterns at 0 GMT March 1st, 2001 over East Asia, TraceP conditions, are shown for errors evaluated using different concentration fields: M (Figure 2.a) and NO_x (Figure 2.b). We notice that both M and NO_x surface criteria refine the region of sharp transition between high concentrations near the continent and the clean area above the ocean, also both criteria refine the areas of high emissions; i.e., above industrial regions in China, Japan, and Korea.

The refinement criteria is applied at simulated hourly increments. Typically, we use one, three, and six hours as the refinement-derefinement (regriding) period.

4.3. S A -D E P G

We start with a numerical investigation of a simplified test to illustrate the solution of advection-diffusion equations with dynamic adaptive mesh refinement using Paramesh. The experimental setting is similar to the one described in (Srivastava et al., 2001b) for the power plant plume. The two dimensional domain covers 400 km in West-East and 120 Km in North-South direction (see Fig. 3). For this experiment the Paramesh grid is set up in the following way. Each Paramesh block is divided in 4×4 grid cells. At the coarse level, each cell covers 10×10 km (10×3 blocks), see Fig. 3.b. At the maximum refinement level (4),

the grid resolution is 1.25×1.25 km (80×24 blocks), see Fig. 3.a. For simplicity we use periodic boundary conditions.

We propose two experiments: (1) a wave that is transported (advected) with constant wind speed through a refined region, and (2) a simulation of atmospheric dispersion of a plume in the atmosphere. The species under consideration in both experiments is HCHO with a background concentration of 8.61E+15 molec/cm^3. The discretization methods for advection and diffusion are described in Sec. 3.

The first experiment shows a wave passing through a refined region. Paramesh performs interpolation and averaging of the solution as the wave passes through interfaces between blocks at different refinement levels. We want to assess whether the wave is distorted by the coarse-fine-coarse interfaces and whether the numerical solution is a good approximation of the exact solution. We consider an initial (semi) cosine profile centered at (60,60) km with a radius of 35 km. The initial profile is transported (advected) for a duration of 16 hours and a wind speed of 5 m/s in the East direction. In Figure 3.a we show the initial profile (towards West) and final solution (towards East) computed on the the finest resolution (1.25×1.25 km). The same experiment is repeated with a coarse resolution (10×10 km), and on a coarse grid with a refined region in the middle of the domain (see the grid in Fig. 3.c).

In Figures 3.b and 3.c we show the relative errors of the coarse and refined grid experiments with respect to the fine solution. Note that the errors in the refined grid solution are slightly smaller, which confirms that the wave is not distorted by passing through the block interfaces. In Figure 3.d we show the West-East slice at 60 km of the solution set at the final time. The fine resolution solution matches the exact solution almost perfectly. The three experiments with different resolutions show that the solution on the Paramesh grid matches the exact solution in this setting.

We next look at dynamic adaptive grids. In the second experiment we consider the dispersion (advection and diffusion) of a plume using the numerical approximation described in Sec. 3 in the above setting. The emission source (of HCHO) is positioned at (62.5,62.5) km and has the rate of 4.67E+23 molec/s and a mixing layer of 1 km. The Eastern wind speed is 5 m/s and the turbulent horizontal diffusivity is 100 m^2/s.

The simulation is carried out for 12 hours. Initially, the source is turned on, but after six hours the emission source is turned off. The plume continues to be dispersed for another six hours. We consider three resolutions: (1) fine resolution throughout the domain (1.25×1.25 km), (2) coarse resolution throughout the domain (10×10 km), and (3) dynamic adaptive resolution based on the curvature criterion (*uptol* =

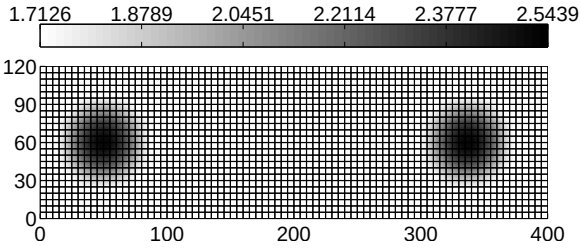

(a) Initial (West) and final (East) solution [1E+16 molec./cm^3]

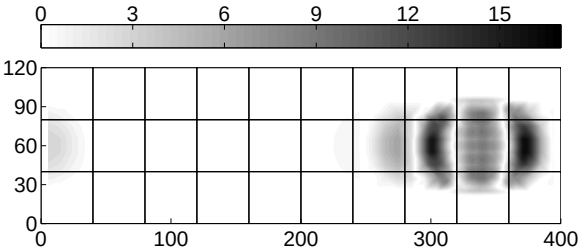

(b) Errors [%] for the coarse grid simulation

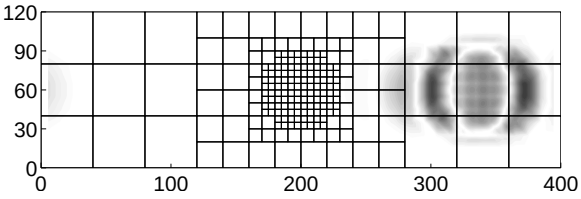

(c) Errors [%] for the refined grid simulation

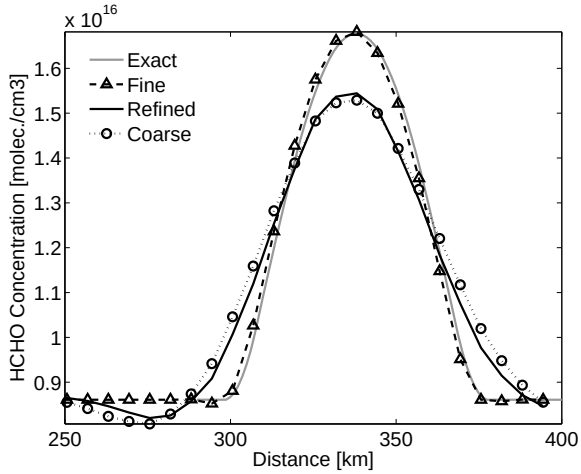

(d) West-East slice at 60 km of the solution at the final time

Figure 3. Wave passing through a refined region. The solution using a refined region is not distorted by the coarse-fine-coarse interfaces. The fine solution on the fine grid is a very good approximation of the fine solution. Each block in (a), (b), and (c) consists of 4×4 grid cells.

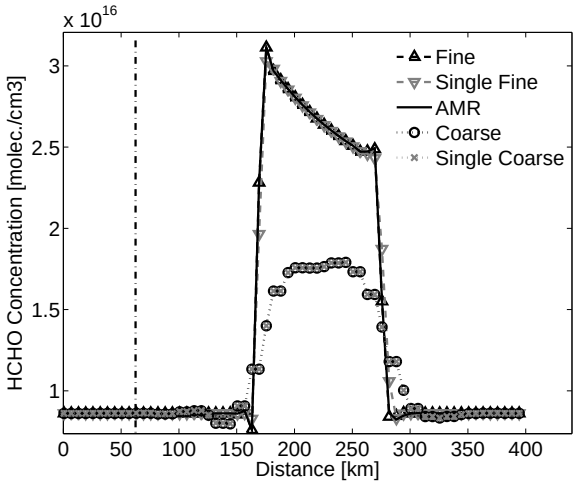

(a) Solution West-East slice at 62.5 km

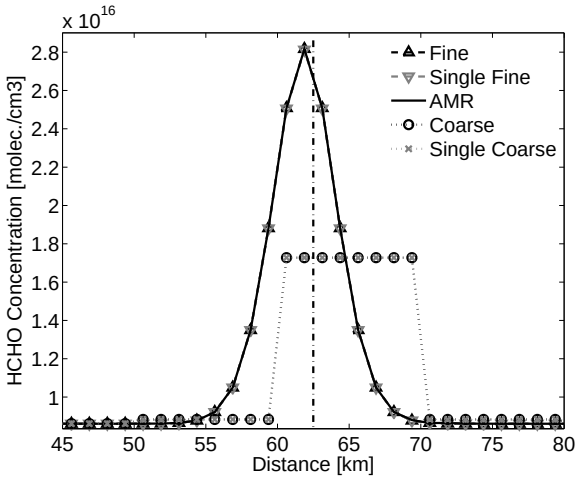

(b) Solution North-South slice at 200 km

Figure 4. Slices of the plume experiment solution at final time (after 12 hours). The solutions using single grids and the ones computed using Paramesh data structures are very similar. The fine resolution solution is very well approximated by the dynamic adaptive mesh solution. The source (denoted by dash-dotted lines) at (62.5,62.5) is turned off after six hours.

0.10 and *lowtol* = 0.01) applied at every step. This adaptive grid moves with the plume. In addition, we consider the fine and coarse resolution experiments on a single grid. This implementation is done outside Paramesh with the purpose of validating the calculations done by Paramesh at block level with the computations done on the entire domain at once.

Figure 4 shows slices of the solution at the final time. We note that the dynamic adaptive grid solution is a good approximation of the fine grid solution using either Paramesh data structures or a single grid. Furthermore, the fine Paramesh and single grid solutions and coarse Paramesh and single grid solutions are very similar, respectively. This shows that the dynamic grid adaptivity does not distort the solution. In Figure 5 we show time snapshots of the the dynamic adaptive grid as it follows the plume dispersion profile – efficiently solving the transport problem. We note that the resolution of emissions should ideally match the resolution of the grid at the source location. This aspect is very important in capturing the solution peaks as seen in Fig. 4.b and can play an important role in the quality of the solution as stated in (Tomlin et al., 1997; Hart et al., 1998).

Figure 4 also shows a typical scenario in which dynamic adaptive resolution is a better strategy than static refinement. The static grid strategy would fix a finer resolution around the source at all times, and a coarse resolution throughout the rest of the grid. As seen in Figure 5.c, if the emissions are turned off, then the fine resolution around the source is no longer necessary; however, fine resolution is necessary while tracking the plume.

In summary, using a controlled simplified experiment, we have shown that using the Paramesh framework (adaptive or static) yields the same result as using a single single grid (without block interfaces). Both static and dynamic refinement do not distort the solution and dynamic refinement yields a good approximation of the exact solution. Moreover, the static refinement around sources is not necessarily the best grid adaptation strategy.

4.4. I C

We next consider the full 3-dimensional model with full chemistry and explain the interface between STEM and Paramesh in detail. This is typical for the way our air pollution model needs to be interfaced to a generic adaptive grid system. During the simulation, data available in STEM-specific data structures need to be copied into Paramesh data structures. The initial conditions consist of initial species concentrations and geographical information that is provided at coarse level at the beginning of the simulation. Meteorological fields, boundary conditions and surface emissions are updated every hour and we refer to these as periodical data. All data are given at the coarse level, except for the emission inventories which are provided at a fine resolution (10×10 Km).

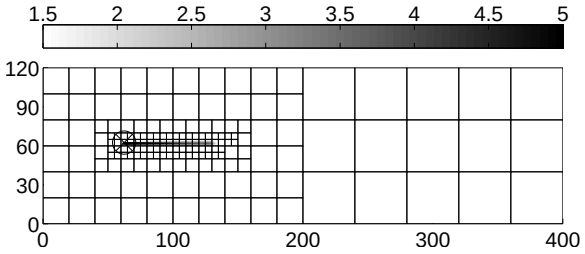

(a) The grid after 4 hours

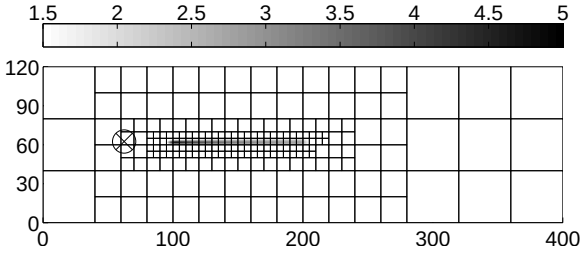

(b) The grid after 8 hours (2 hours after source shutoff)

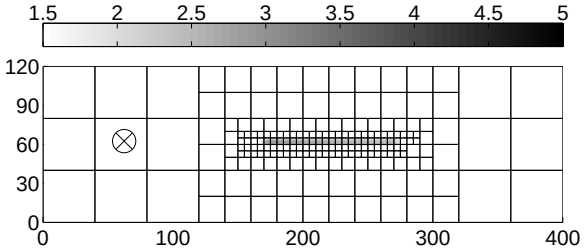

(c) The grid after 12 hours (final time)

Figure 5. The dynamics of the grid adaptivity for the plume experiment. Fine grids follow the plume profile as it is dispersed. The source (located at the crossed circle) at (62.5,62.5) is turned off after six hours.

The meteorological fields need to be interpolated to each block's refinement level since they are provided at coarse level from an offline meteorological simulation and data assimilation. Surface emissions are averaged, if necessary, to each working block's refinement level; they are not stored as Paramesh variables.

The domain lateral boundary conditions are treated separately, just like the emission data and supplied to Paramesh during computation upon request. Experimentally, we noticed a loss in accuracy associated with block refinement near the physical boundary due to the fact that boundary data are coarse and consist in a single layer. Since high resolution lateral boundary conditions are not available, the blocks neighboring the physical boundary are kept at the coarse level. This

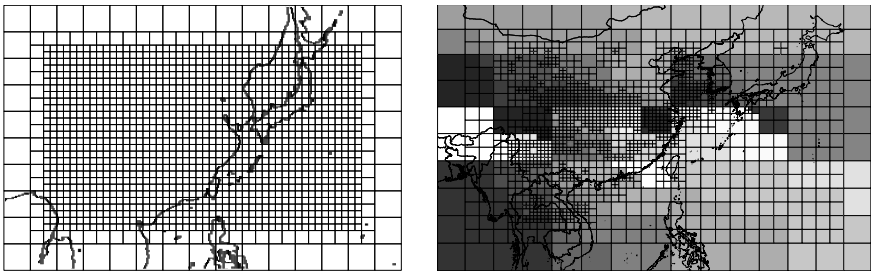

(a) (b)

Figure 6. (a) Fine grid layout (only blocks are shown) for level 3 with the boundary restriction applied. (b) Mapping of adaptive level 4 grid blocks onto 32 processors based on Morton ordering. Each processor is marked with a different shade of gray.

restriction also affects the next inward layer of blocks that cannot be refined with more than one level than their neighboring blocks, and so on. This is of no concern since in our case little chemical activity involving pollutants takes place near the physical boundary. All the blocks affected by this restriction will be no more than two coarse blocks "distance" from the physical boundary. Figure 6.a shows the fine grid layout for level 3 (everything refined) with the boundary restriction applied.

We note that the influence of the lateral and top boundary conditions is felt throughout the domain for long simulations. In our case we keep the boundary mesh points resolution at the coarse level - this may generate errors that will accumulate and give unsatisfactory results for long runs. The uncertainties associated with artificial boundary conditions may override the advantages of adaptive resolution.

Another aspect related to our implementation is that the time integration is performed with the smallest step size appropriate for all the blocks; i.e., the step size chosen for the finest level of refinement is used even for the coarse regions which is typically not necessary. We have developed a suitable approach for the time integration that considers the refinement level for each block and applies an appropriate timestep (Constantinescu and Sandu, 2007; Sandu and Constantinescu, 2007). Another approach based on conservative symmetric Strang splitting is discussed in (Odman and Hu, 2007).

4.5. P A

Paramesh maps the blocks onto processors using a space filling curve technique, Morton ordering, such that neighboring blocks are mapped onto the same processor. This approach reduces the amount of inter-

processor communication needed to fill in the guard-cells at each iteration. The mapping process is handled by Paramesh and is transparent to the user. Figure 6.b shows the mapping of the STEM variables onto 32 processors for the grid adaptively refined to level 3.

The regriding process is handled by Paramesh at the user request. Each time the regriding is performed, blocks on each processor are refined or derefined according to a criterion and then migrated to other processors in order to balance the processor workload, if necessary.

It should be noted that the vertical coordinate is expressed in sigma–altitude coordinates and in this work the topography is interpolated. In general, a vertical interpolation of the concentration fields is needed for high resolution data since large local variations in topography have a large impact on the levels in the sigma–altitude coordinates.

Lateral boundary conditions and emission data are broadcast to all processors every simulated hour since the Paramesh version that has been used in our experiments does not provide support for managing boundary data. The communication cost and memory requirements are not significant relative to each processor's workload. The alternative for broadcasting would be to implement a parallel data I/O management routine. This routine would monitor Paramesh block migration and distribute the boundary conditions and emission sources in sync with Paramesh block migration. Such an approach is not considered for this study.

5. Results

In this section we present the numerical results for the adaptive mesh refinement approach used in the atmospheric chemical and transport model STEM. We begin with a description of the experimental setting. In Sec. 5.2 we discuss several aspects related to refinement criteria. Then we investigate the benefit of using a dynamic mesh refinement approach as opposed to a static refinement (adaptive refinement done only at the beginning of the simulation window). The regriding frequency is also ascertained. In Sec. 5.5 we present some accuracy results for the selected refinement approaches and in Sec. 5.6 we analyze the parallel performance of our approach.

5.1. E S

The test problem is a simulation of air pollution in East Asia. The meteorological fields, boundary values, and emission rates correspond to the NASA TRAnsport and Chemical Evolution over the Pacific

(TraceP) field experiment scenarios (Carmichael et al., 2003) starting at 0 GMT of March 1^{st}, 2001. The simulated region covers 7200×4800 Km. The meteorological fields are given by the dynamic meteorological model RAMS (Pilke et al., 1992). The initial fields and boundary conditions correspond to TraceP data campaign. The tests use 4 levels of refinement from the (STEM) nominal horizontal resolution of 80×80 Km (level 1) down to 10×10 Km (level 4). At the coarse level there are 15×10 blocks containing 6×6 cells, at level 4 there are 5058 working blocks which amount to 182,088 mesh points. Each mesh point holds a column of 18 layers of STEM variables, 2340 in total per Paramesh mesh point; these include meteorological, topographical data, and species concentration corresponding to a specific column. The number of variables for the fine simulation totals to about 0.45 billions. Each layer in a column holds 102 chemical species concentration out of which all are transported (advection + diffusion) and 93 are considered in the chemical reactions. The emissions inventory consists of yearly averaged estimates. The hourly emission rates are weighted based on a daily estimated distribution. Stronger emission rates during day-time and early evening hours and weaker during early morning hours.

The simulations have been performed on System X computer cluster which is one of the fastest academic supercomputer in the world at 12.5 TFlops. System X has 1100 node Apple XServe G5 dual processor, 4 Gb of RAM per node. The interconnect consists of InfiniBand switches (primary) and Cisco 4506 Gigabit Ethernet (secondary).

The simulation timings varied with the cluster loading and for this work we used the total number of blocks as a measure of the total computational workload. For this purpose, the regriding and guard-cell filling overheads can be ignored since this application is very computationally intensive and the regriding interval is relatively large compared with the time step (see Sec 5.4). The workload is similar for all blocks and the blocks are quasi-equally distributed on all processors, and thus, the total number of blocks can be a fair measure of the total workload. Our experiments use a range of processors spanning from 8 to 96 which take 16 to 36 hours of real time to simulate one week.

Accuracy is tested against a reference solution obtained by a refinement of the entire domain to level 4. The computational resources prohibit us to go any higher for these experiments. The simulations correspond to the period between 0 GMT of March 1^{st}, 2001 and 0 GMT of March 8^{th}, 2001.

5.2. R C

In this section we discuss particular aspects of the refinement criteria. We begin our experiments with the criterion set on the O_3 curvature. Unfortunately, this approach did not bring significant improvement to the O_3 error estimates during our simulations as one would expect. This is most likely due to the numerical error propagation of poorly resolved ozone chemical precursors through the chemical process to the O_3 formation. The criterion set on O_3 solely will not be analyzed in the reminder of this paper.

High resolution emissions (e.g., NO, NO_2, HCHO) have a large impact on the O_3 field, and thus, they should be accounted for in order to accurately predict the actual O_3 concentration. The inclusion of the ozone chemical precursors (e.g., NO_x, HCHO) in the refinement criterion may give us a better accuracy for the ozone concentration field. The thresholds for the refinement-derefinement criterion (*lowtol* and *uptol*) also have a strong effect on the accuracy of the ozone concentration field. They control the amount of refinement for a given criterion. Moreover, they directly control the computational workload. For the rest of the paper we mainly focus on the combined species criterion *M* and NO_x. Both have been discussed in Section 4.2.

Intuitively, the *M* criterion considers both the O_3 precursors which are introduced in the domain mainly through emissions. High ozone concentration field may be present in regions that are downwind of the emission sources due to the advection processes. The NO_x criterion accounts only for two of the O_3 precursors.

5.3. G D - S . D

In this section we discuss the differences between the static and dynamic grids. We begin by looking at the grid dynamics over time. Throughout this section, the reference (fine) resolution is limited to level 3.

A major factor in the grid layout based on one of our criteria is the diurnal cycle. During this cycle both the intensity of solar radiation received by each layer and the rate of surface emissions change. A secondary factor is generated by the transport mechanism (advection) that carries sharp gradients across the domain. The sharp gradients are associated with large discretization errors. The grid layout is affected by a combination of the two factors which lead to a grid dynamics that is relatively localized due to emissions and non-periodic due to advection and the meteorological fields. These assumptions are confirmed by our experiments. At least in theory, these facts favor the use of dynamic versus static grids.

Static and dynamic grids have both advantages and disadvantages. Static non-uniform grids involve less work with regriding but a larger overhead in workload in order to cover a similar surface that a dynamic grid would cover. In other words, the static grid might use a very refined mesh on a smooth solution that could be solved using a coarser grid with insignificant loss in accuracy. On the other hand, the dynamic grids may be more efficient in managing the workload but have the downside of extra overhead associated with the regriding operation; moreover, as discussed in (Odman and McRae, 2003), the dynamic grids have the potential to capture solution features that are not captured by the static grids. In their study it is shown how the static grids predict a peak which is not present in the dynamic grid simulation or measurements.

A direct comparison between the two approaches is difficult to make because of factors that may not be quantifiable. First is the human error factor, the person (in the case it is not done automatically) that positions the static grid may be more or less experienced, it should be noted that this factor can be completely avoided using dynamic grids. In the AMR approach the refinement criterion has a very important role as its parameters can highly influence the accuracy for a targeted set of species. Other factors might be the refinement-derefinement interpolation order or hidden chemical reactions that may count more than others toward some reference species. This aspect can also be included in the AMR framework through the refinement criterion. For illustration purposes, in Figures 7 and 8, we present the grid dynamics for the NO_x refinement criterion with high refinement tolerances (i.e., small number of refined grids). In Figure 7 we show the grid dynamics during 24 hours, for every six hours. Note that the grid has noticeably changed during one day over the center of the domain which is the area of interest for us (especially from panel (a) to panel (d)). Figure 8 represents the same simulation 24 hours apart. Specifically, Figures 7.a, 8.a, 8.b represent the grid at the same time on consecutive days.

As expected there is no emerging pattern. The grid changes at least every six hours (our saved data interval), is relatively localized, but atypical refined grids emerge in previously unrefined regions as well as fine grids are brought to a coarser level. We remark that in all our simulations the solution has a transient of about 2-3 days, which is also illustrated in Figures 7 – 8. As the simulation progresses, the solution becomes smoother and the error estimators allow the grid to be coarser. Moreover, the transient phase might be caused by the fact that initial data are not given at high resolution. This effect has also been noticed and addressed in (Srivastava et al., 2001b). An initial

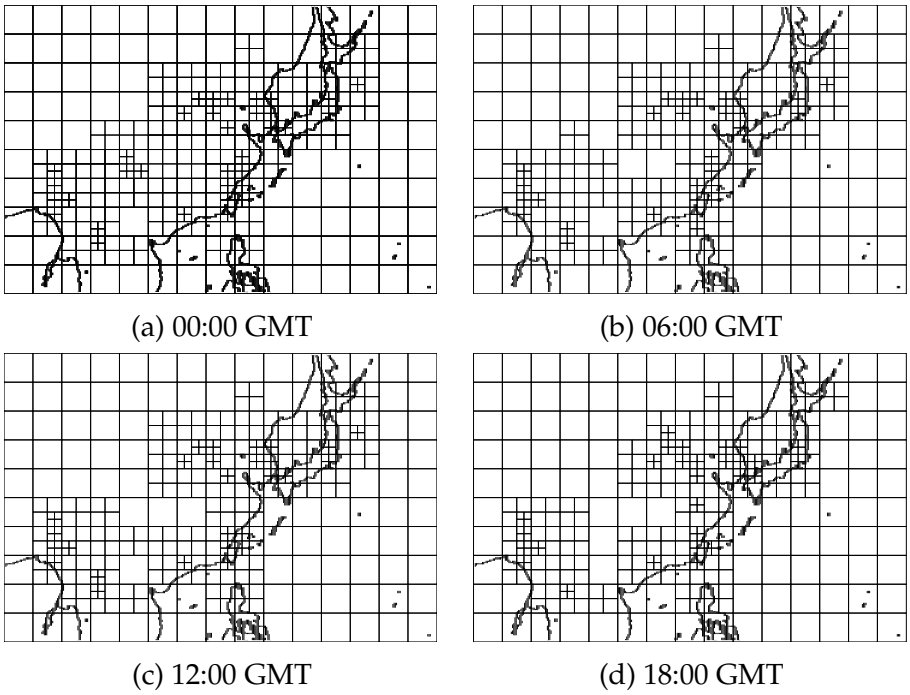

(a) 00:00 GMT (b) 06:00 GMT

(c) 12:00 GMT (d) 18:00 GMT

Figure 7. Grid dynamics for *M* refinement criterion. Each snapshot is taken 6 hours apart starting with 1st March 2001 - 6:00 GMT: (a) 00:00 GMT; (b) 06:00 GMT; (c) 12:00 GMT; (d) 18:00 GMT.

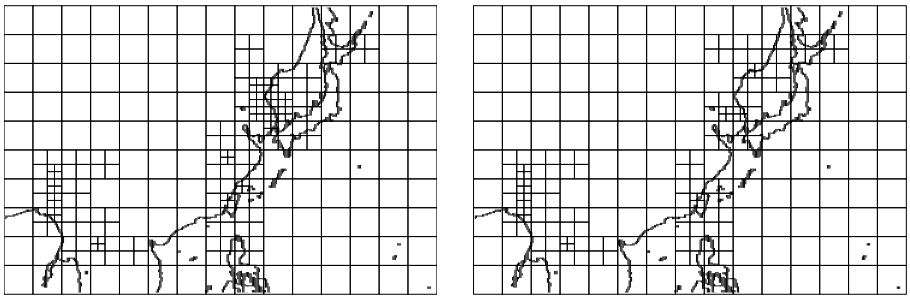

(a) 2nd March 2001 (b) 3rd March 2001

Figure 8. Grid dynamics for *M* refinement criterion. Each snapshot is taken 24 hours apart starting with 2nd March 2001 - 0:00 GMT: (a) 2nd March 2001 - 0:00 GMT; (b) 3rd March 2001 - 0:00 GMT.

"preadaptation" step is proposed that refines the grid in regions with large concentration gradients.

5.4. R I

Paramesh is not equipped with a facile mechanism to accommodate for a buffer region as described in Berger and Oliger (1984) (i.e., refine a larger area surrounding the actual flagged region) in order to avoid frequent regriding. Even if the refined grid is relatively localized due to the diurnal cycles, the concentration fields may shift through advection; however, through the presence of NO_x or HCHO, new O_3 is created during day-time above regions with high emission rates. Regriding frequency is analyzed next.

Ideally, without considering the interpolation errors and the computational overhead, we should refine every three minutes (STEM - time step length) or we may try to minimize the computational overhead due to regriding and refine every 24 hours. If the regriding operation takes place too often, a large overhead is incurred relative to the execution time. If regriding is performed too seldom, together with the fact that a refinement buffer region is not considered, the species distribution will have changed so much that the grid layout would be inadequate for reducing the numerical errors with the evolved solution.

In order to analyze the optimal regriding frequency and to assess the use of dynamic AMR versus the static approach, we choose the following scenarios: a static scenario with comparable (or slightly larger) workload than AMR and dynamic AMR scenarios with regriding intervals of one, three, and six hours. The workload for the above mentioned scenarios is shown in Figure 9.a. The one hour refinement frequency is considered the reference. Refining more often would probably not be justified by the solution dynamics. The total number of blocks for the three hour refinement frequency scenario follows closely the one hour scenario.

We now show a comparison between an AMR static run and a dynamic AMR with the workload, expressed in the number of blocks, shown in Figure 9.a. The workload for both scenarios is similar in terms of the number of gridpoints and we consider the same refinement criterion, NO_x. In Figure 10 we show the vertically averaged O_3 numerical errors after two simulated days for the coarse, static and the one and six hour regriding interval dynamic AMR scenarios. In this case, static and dynamic refinement seem to have similar performance in terms of accuracy. Although, the AMR approaches show a slight advantage.

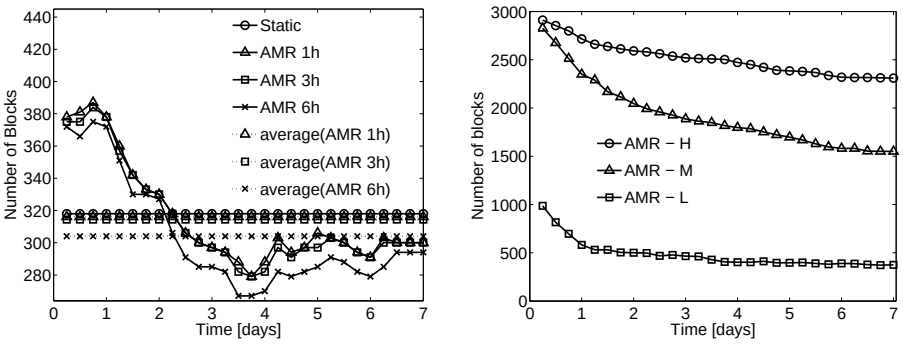

(a) (b)

Figure 9. Total block count evolution for one week: (a) Criterion NO_x with a static grid and one, three, and six hours regriding interval, together with their mean values (approximation of their workload) and (b) three AMR scenarios with level 4 refinement.

Larger improvements are expected for finer grids as the versatility of the AMR approach can be better exploited and high resolution data (e.g., emissions in our case) will have a broader impact on the accuracy of the simulation. We note that emission rates have a diurnal cycle and a weekday-weekend variation; moreover, sporadic events like biomass burning (e.g., forest fires) or volcano eruptions require dynamic grid adjustments for effective solution resolution. Furthermore, the pollution episode changes due to the influence of the meteorological fields.

Based on the workload results and on the fact that we capture both diurnal and nocturnal cycles with good accuracy, for the rest of the paper, we consider the three hour refinement interval for all AMR simulations. This interval seems to provide a good trade-off between efficiency and accuracy.

5.5. A I

Here we analyze the performance of our AMR approach. For numerical exemplification we consider three AMR scenarios based on the *M* criterion with different refinement-derefinement tolerances: a heavy load – AMR-H, a medium load – AMR-M, and a light load simulation – AMR-L. The tolerances for each scenario are given in Table I.

The number of blocks is used as an approximation to the computational effort. The actual number of blocks we measure during the simulations presented in this section are shown in Figure 9.b. Note that the coarse (level 1) has 150 blocks and the reference level 4 has 5058 blocks. We perform a one week AMR simulation. Our reference

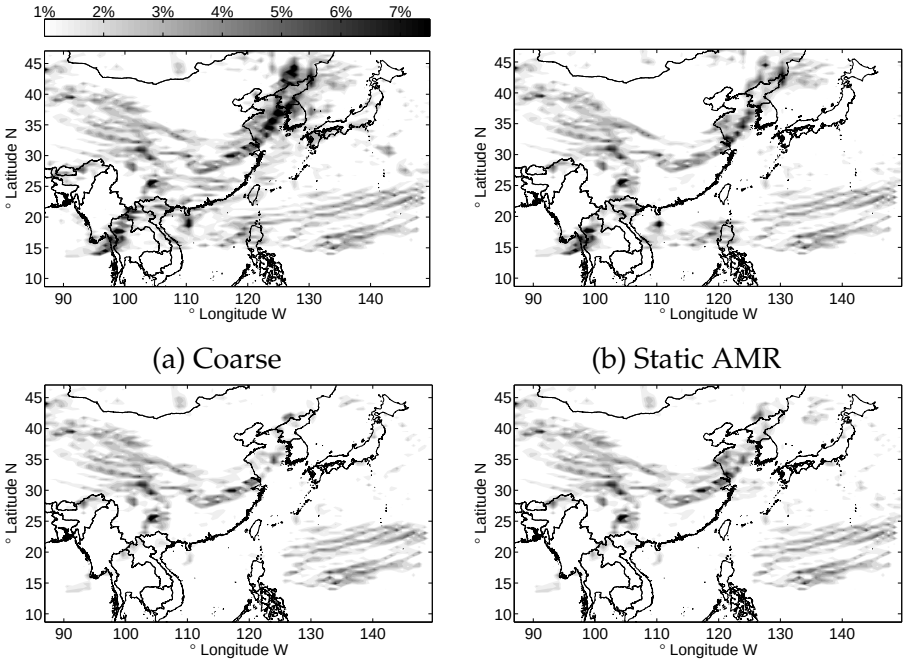

Figure 10. Vertically averaged O_3 numerical errors (in percent) after two simulated days at 0 GMT for (a) the coarse resolution, (b) static grid (refined at the beginning of the simulation), and dynamic AMR with (c) one hour and (d) six hours regriding interval using the error control based on NO and NO_2 fields curvature. The reference (fine) level is 3.

solution is at level 4 (10×10 Km per gridpoint). The criterion used in our tests is M. The four species provide the error control mechanism for the adaptive refinement criterion in order to improve the accuracy of the ozone concentration field.

In Figure 11 we present the coarse and AMR O_3 and NO vertically averaged relative (numerical) errors with respect to the fine grid solution after one simulated week. The AMR performs better than the coarse simulation especially above areas of intense activity above China, Korea, and Japan where the grid is predominantly refined and the emission sources are treated at or close to the fine resolution. Note that the error levels are elevated on the Eastern part of the domain. This also corresponds to the downwind direction. This downwind error points at the emission sources errors in the China, Korea, and Japan that get amplified by the chemistry and transported by the advection.

In the above results AMR-H has a very high accuracy performance for both species, while AMR-L has not performed so well. This sug-

Table I. Refinement and derefinement tolerances for three selected AMR scenarios using the multiple species refinement criterion on *M* based on their field curvature Timing for fine, coarse and three AMR cases for one simulated week.

Simulation type	*lowtol*	*uptol*	Time [s]	Average gridpoints
Fine	-	-	429,299	36×5058
AMR-H	0.075	0.350	126,697	36×2548
AMR-M	0.100	0.350	85,020	36×1990
AMR-L	0.200	0.450	20,526	36×532
Coarse	-	-	4,150	36×150

gests that insufficient refinement does not bring any significant gains in terms of accuracy. The meshpoint dynamics over the one week period is shown in Figure 9.b. As we have expected, the system finds itself in a relative steady state - fine grids may move but the overall number of meshpoints is kept relatively constant, decreasing slowly as the solution becomes more and more smooth. We note that different criterion tolerances may lead to different fine grid distribution over long simulations. AMR-H has a almost perfect fit with the reference (fine) solution and AMR-L with the coarse solution.

In Figures 12 – 14 we present the O_3, NO, and HCHO predicted concentration evolution over one week at ground level for Beijing, Seoul, Shanghai, and Tokyo using the coarse, AMR-M (i.e., medium load scenario), and fine simulations. The concentration fields are sampled every six hours. Figure 12 shows the O_3 expected concentration over the four cities. We notice a good prediction for AMR after the first two days when the transient phase is over. The NO (Fig. 13) and HCHO (Fig. 14) concentration fields have the same pattern as for O_3. The effect of using high resolution emissions is visible in the HCHO evolution which shows spurious peaks for the coarse scenario; however, the AMR solution is not corrupted. This translates directly in the fact that higher emissions lead to a finer grid and thus, a better overall accuracy.

We note that the day two Shanghai coarse simulation under-predicts the NO peak (Fig. 13.c) and over-predicts the HCHO one (Fig. 14.c). The primary reason for this effect is due to the coarse mode simulation spreading the emissions over too broad a region. As a result, the primary emissions increase too soon during a strong continental front passage. The high levels of NO_x, CO, and HCHO along with

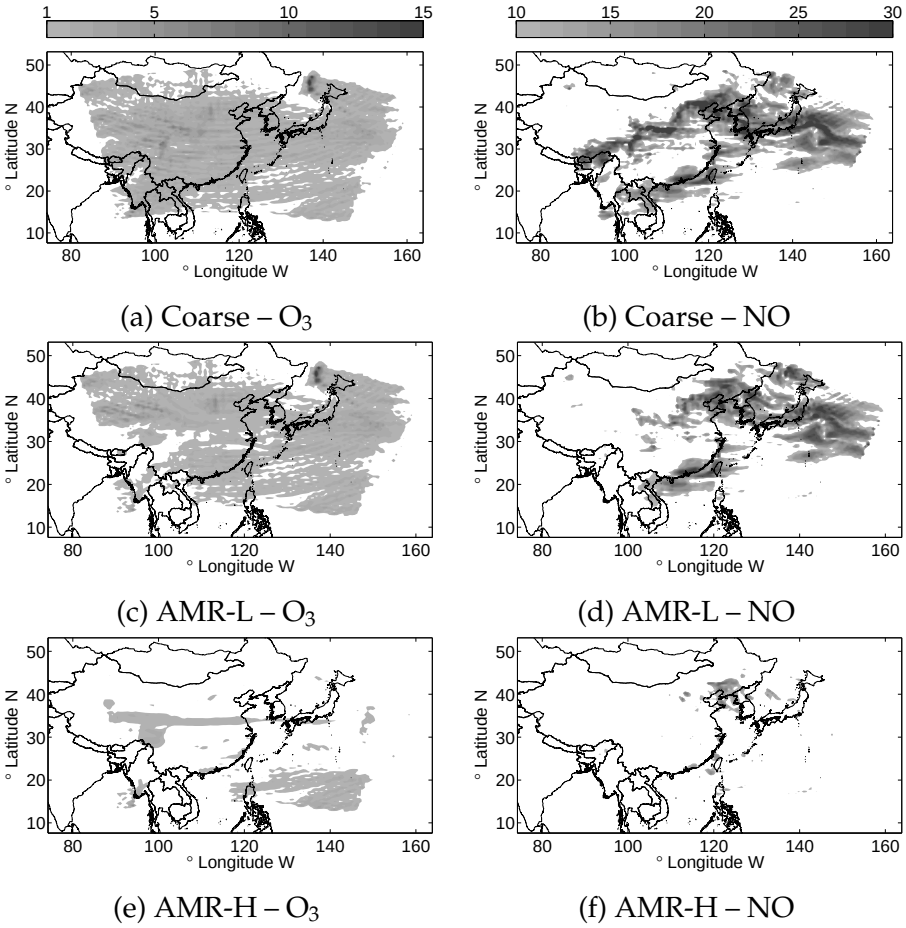

Figure 11. Vertically averaged O_3 and NO errors (in percent) after one week of simulation ending at 0 GMT of March 8^{th}, 2001, for: (a, b) – coarse, (c, d) – AMR-L, and (e, f) – AMR-H. The maximum refinement level is 4 (10×10 Km). The reference (fine) level is 4.

reduce photolysis rates have a net effect on the chemistry in the coarse simulation leading to a reduction in O_3 and a shift in the partitioning in NO_x to higher NO2 and lower NO. These results show the complex coupling between resolution, emissions, and chemistry.

5.6. P I P T

In this section we investigate the efficiency of our approach. We start by looking at the timing results for the AMR scenarios discussed in the previous section. We continue to analyze the parallel performance for a simplified case.

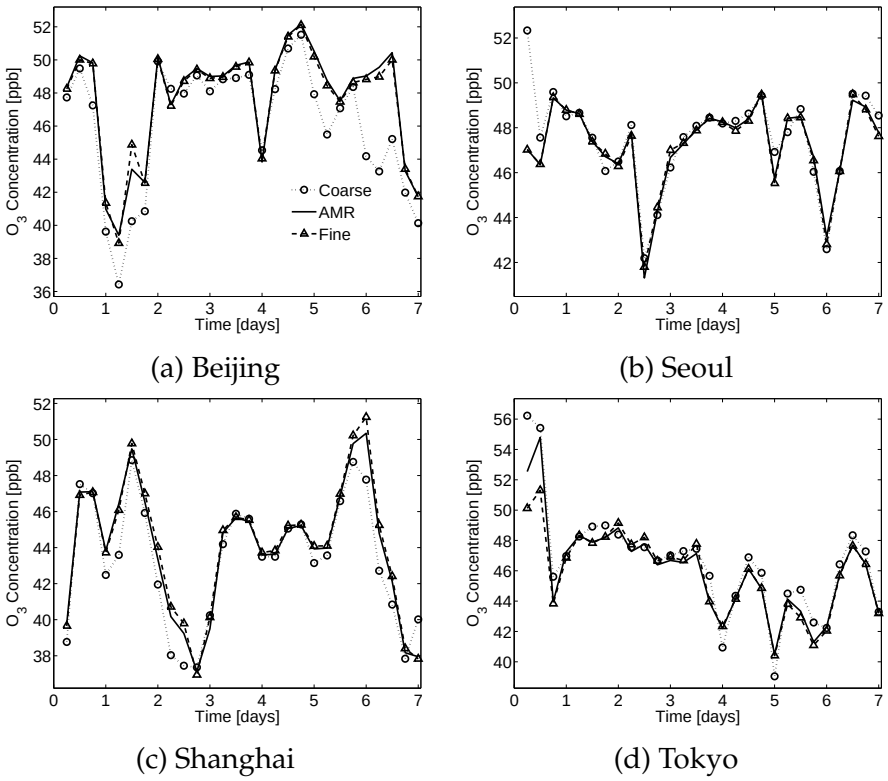

Figure 12. Simulated O_3 concentration during one week at ground level at: Beijing, Seoul, Shanghai, Tokyo. The refinement criterion is *M* (AMR-M).

Table I shows the wallclock for several scenarios: Fine, Coarse, and three AMR runs, for one simulated week. The application tuning for specific processor workload is a problem in itself, especially for parallel implementations due to the difficulty in managing the amount of refinement that each processor does. Scenario AMR-H is close to a quarter of the total fine wallclock and close to our expectations in terms of accuracy as shown in the previous section. AMR-L is very competitive in terms of timing but the accuracy of the simulation is degraded. In our experiments we noticed that accuracy is tightly linked to the number of meshpoints that are concentrated in the higher estimated error areas.

For the parallel performance tests we consider the timing results for one simulated hour at the finest refinement level on 16, 32, 64, and 96 processors. These results are presented in Table II. Communication-wise, for 16 processes we have few processors exchanging large amounts of data while for 96 processes there are many processors exchanging a

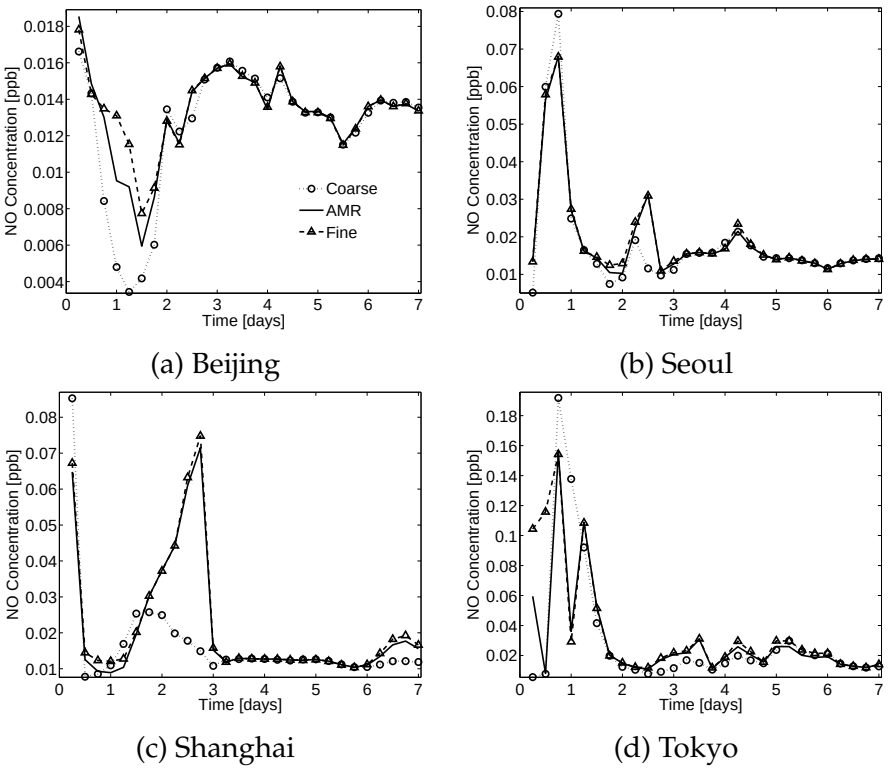

Figure 13. Simulated NO concentration during one week at ground level at: Beijing, Seoul, Shanghai, Tokyo. The refinement criterion is M (AMR-M).

small amount of data. Note that we have a super scalar speedup for 32 processors (2 proc./node); this is probably due to the cumulative effect of good data locality and cache efficient data size.

Considering the fact that the workload remains constant, the speedup is relatively good especially when using one processor per node. As expected, the computationally intensive part of our application shows an insignificant improvement when we switch from one to two processors per node. On the other hand, the communication intensive part which consists in guard-cell filling shows a large improvement when switching from two to one processors per node. The reason for that is probably a less congested communication pattern, at least on the secondary interconnect level.

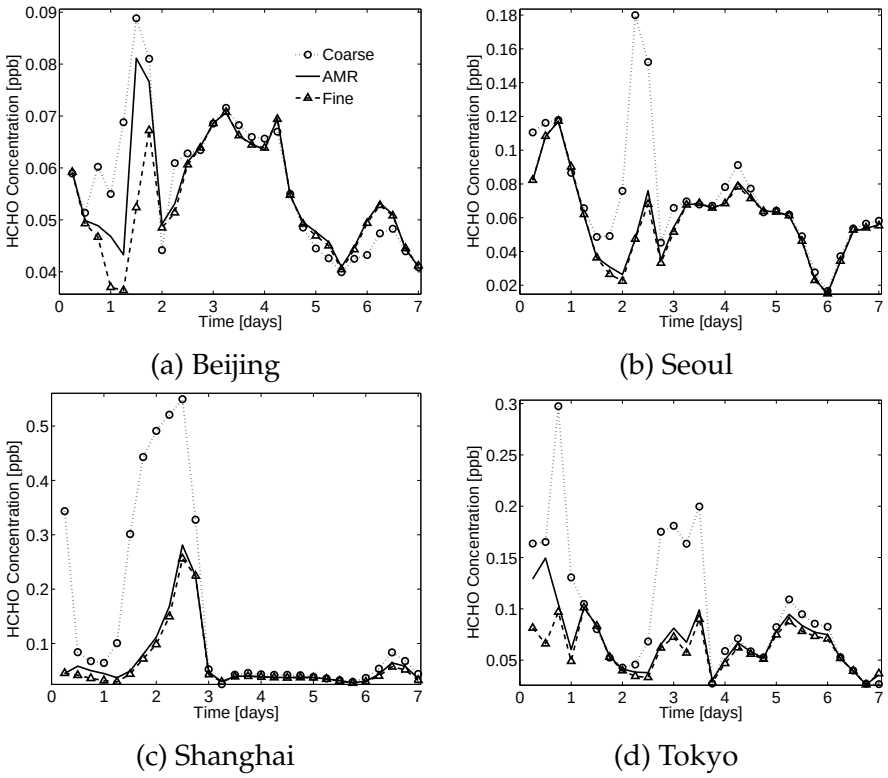

Figure 14. Simulated HCHO concentration during one week at ground level at: Beijing, Seoul, Shanghai, Tokyo. The refinement criterion is M (AMR-M).

Table II. The wallclock for one hour of simulated time on the finest refinement level (4) when using one or two processors per node. The ideal timing is shown in parenthesis.

No. of Procs.	Time [s] 1 proc./node (ideal)	Time [s] 2 proc./node (ideal)
16	2163(-)	2739 (-)
32	1125 (1081)	1270 (1369)
64	841 (540)	1206 (684)
96	502 (270)	816 (342)

6. Conclusions and Future Directions

In this paper we present an application of adaptive mesh refinement approach to regional air quality modeling. Insufficient grid resolution is known to cause considerable loss of accuracy. Adaptive mesh refinement can correct this by estimating numerical errors and automatically placing additional resolution where needed. Various studies focused on the (static) nested grids or stretched grids (see Sec 2) but fully dynamic AMR for chemical and transport models has not been intensively explored in the past. In this manuscript we extend the previous work and propose new research avenues.

The adaptive mesh management is implemented using the generic tool Paramesh. This allows transparent use of grid operations like refinement and data interpolation, and allows for immediate parallelization of the system. The adaptivity criteria include the curvature of the NO_x, HCHO, and of the O_3 concentration fields. Based on user imposed error tolerance levels, one can vary the workload and runtime to obtain better accuracy for some species. Experimentally, the criterion set on O_3 errors performed poorest with respect to O_3 accuracy, and hence, we ruled out O_3 alone as a refinement criterion. Our numerical results point to a criterion based both on O_3 and its chemical precursors, especially NO_x and HCHO. The multiple (weighted) species criterion yields the best results. In this work we consider only the field curvature for the error estimation. We plan to investigate criteria based on other error estimation approaches like gradient or numerical truncation error in future studies.

Numerical tests are performed for an air pollution simulation in East Asia in March 2001. The data correspond to NASA's TraceP experiment. All numerical tests show an increased accuracy with mesh refinement, as expected. The computational workload is also increased, but remains considerably smaller than the workload needed by a complete refinement of all the domain.

In this paper we consider 2D (horizontal) adaptivity for the 3D air pollution simulations. Full 3D adaptivity was shown to be advantageous in local air pollution modeling by Ghorai et al. (2000), but has not been extensively studied for regional-to-global models. Full 3D adaptivity is possible but more complicated. For example, the radiation code computes the radiation levels at multiple wavelengths based on the concentrations of different species along each column, and based on the location of the column and time of day. The photolysis rates at each level are then computed based on these radiation levels. If different refinement levels are used at different heights along the same vertical column then these computations become more involved. One possible

approach is to compute the column concentrations and photolysis rates at the coarsest level, then interpolate them to the corresponding fine levels.

In our scenarios a transient phase seems to be unavoidable. This phase is characterized by a very fine grid at the beginning of the simulation (first two days). The fine grid gradually converges to a steady state in terms of the number of gridpoints. This transient phase is probably due to the fact that the initial data have a coarse resolution. Special care should be taken about the refinement tolerances, since in the beginning of the simulation the grid may be refined more than it should with respect to the entire simulation time. The main restriction in this field of study is the computational resources, so if one would like to keep using constant resources the transient might cause some problems. A restart approach could be taken: One could restart the application after the transient has ended. Alternatively, an application wide refinement approach needs to ensure that the total workload is under control throughout the simulation interval.

A regriding period of three hours is a good trade-off between accuracy and regriding overhead. Moreover, our experiments show that a three hours regriding interval leads to a similar number of meshpoints as for a one hour refinement interval and also accounts for the diurnal cycle with good accuracy. An open problem is the optimal choice of the criterion tolerances and weights. These can be approximated in such a manner that the total number of points do not exceed the available resources or allotted simulation time. The weights that are assigned to species in mixed criteria can potentially be determined through sensitivity analysis.

The dominant errors are located downwind of the emission sources. A possible cause is the effect of errors in regions with high emission rates that are amplified by the chemical processes and advected by transport equations. This aspect would suggest a refined grid (increased resolution) upwind of the area of "interest". This fact favors the use of dynamic AMR since meteorologic fields change with time and the upwind direction changes as well.

In this paper the same time step is used for all meshpoints regardless of their resolution (refinement level). In terms of efficiency, a lot of CPU time is lost for the time integration of coarser blocks with the time step length suited for the finest resolution. This will be avoided by implementing a multi-level time integration which is currently under study (Constantinescu and Sandu, 2007).

Another aspect that could improve the efficiency of our application is the use of parallel input/output. For now, we let the master process read all the initial and periodical data and distribute it among the

slaves. When using a small number of processors does not have a large impact on efficiency, but does not scale well to a large number of processors.

In our current setting the meteorological data consists of RAMS produced fields that were analyzed through data assimilation. These fields were produced at a fixed resolution. They correspond to the coarsest resolution of the adaptive mesh. The fields are interpolated down to the computational resolution. A better approach would be to have the fields calculated and assimilated at the finest resolution, and then averaged to obtain the corresponding fields at coarser resolutions. Yet another approach would be to compute the meteorological fields with the same spatial and temporal resolution as the air quality model as suggested in (Odman et al., 2000; Odman et al., 2002); this implies that the air quality model and the meteorological model run in coupled mode and use the same (adaptive) grid. This tight coupling ensures consistency, and allows the grid to be adapted based both on meteorological variables and tracer concentrations; but in the same time, it makes it difficult to assimilate the meteorological observations independently. Computing the meteorology on a distributed system could in fact save computational time, as reading the same large amount of data from a file and distributing it periodically tends to be expensive and is a bottleneck for the computational algorithm.

We note that the dynamic adaptive mesh refinement approach can be extended to global air quality models. In this case, the absence of boundary conditions is advantageous for the AMR framework conveying more freedom for fine grid placement. The automatic grid adaptivity in time can (automatically) integrate any sporadic event in an online fashion. The advantages are evident in operational or critical systems.

Acknowledgements

This work was supported by the National Science Foundation through the awards NSF CAREER ACI 0093139, NSF ITR AP&IM 0205198, and CCF-0515170. Our special thanks go to Virgina Tech, Laboratory for Advanced Scientific Computing and Applications for the use of the Anantham and System X clusters.

References

Berger, M. and J. Oliger: 1984, 'Adaptive mesh refinement for hyperbolic partial differential equations'. *Journal of Computational Physics* **53**, 484–512.

Borthwick, A., R. Marchant, and G. Copeland: 1998, 'Adaptive hierarchical grid model of water-borne pollutant dispersion'. *Proc. 1st Int. Conference on Industry, Technology and Environment (ITE'98), Moscow, Russia* pp. 11–16.

Boylan, J., M. Odman, J. Wilkinson, A. Russell, K. Doty, W. Norris, and R. McNider: 2002, 'Development of a comprehensive, multiscale "one-atmosphere" modeling system: application to the Southern Appalachian Mountains'. *Atmospheric Environment* **36**(23), 3721–3734.

Carmichael, G.: 2003, 'STEM – A second generation atmospheric chemical and transport model'. *URL: http:// www.cgrer.uiowa.edu*.

Carmichael, G., Y. Tang, G. Kurata, I. Uno, D. Streets, J. Woo, H. Huang, J. Yienger, B. Lefer, R. Shetter, D. Blake, E. Atlas, A. Fried, E. Apel, F. Eisele, C. Cantrell, M. Avery, J. Barrick, G. Sachse, W. Brune, S. Sandholm, Y. Kondo, H. Singh, R. Talbot, A. Bandy, D. Thorton, A. Clarke, and B. Heikes: 2003, 'Regional-scale Chemical Transport Modeling in Support of the Analysis of Observations obtained During the Trace-P Experiment'. *Journal of Geophysical Research* **108**(D21 8823), 10649–10671.

Carter, W.: 2000, 'Implementation of the Saprc-99 Chemical Mechanism Into The Models-3 Framework'. Technical report, United States Environmental Protection Agency.

Chock, D., S. Winkler, and P. Sun: 2002, 'Effect of grid resolution and subgrid assumptions on the model prediction of non-homogeneous atmospheric chemistry'. *The IMA volumes in mathematics and its applications: Atmospheric modeling, D.P. Chock and G.R. Carmichael editor* , 81–108.

Constantinescu, E. and A. Sandu: 2007, 'Multirate timestepping methods for hyperbolic conservation laws'. *To appear in Journal of Scientific Computing*.

Damian, V., A. Sandu, M. Damian, F. Potra, and G. Carmichael: 2002, 'The kinetic preprocessor KPP - a software environment for solving chemical kinetics'. *Computers and Chemical Engineering* **26**, 1567–1579.

Ghorai, S., A. Tomlin, and M. Berzins: 2000, 'Resolution of pollutant concentrations in the boundary layer using a fully 3D adaptive technique'. *Atmospheric Environment* **34**, 2851–2863.

Hart, G., A. Tomlin, J. Smith, and M. Berzins: 1998, 'Multi-scale Atmospheric Dispersion Modelling by Use of Adaptive Gridding Techniques'. *Environmental Monitoring and Assessment* **52**(1-2), 225–238.

Khan, M.: 2003, 'Development and application of an adaptive grid air quality model'. Ph.D. thesis, Georgia Institute of Technology, School of Civil and Environmental Engineering.

MacNeice, P. and K. Olson: 2003, 'PARAMESH V4.0 – Parallel Adaptive Mesh Refinement'. `http://www.physics.drexel.edu/~olson/paramesh-doc/Users_manual/amr.html%`.

MacNeice, P., K. Olson, and C. Mobarry: 2000, 'PARAMESH: A parallel adaptive mesh refinement community toolkit'. *Computer Physics Communications* **126**, 330–354.

Odman, M. and Y. Hu: 2007, *Air Pollution Modeling and Its Application XVII*, Chapt. A Variable Time-Step Algorithm for Air Quality Models, pp. 411–420. Springer US.

Odman, M., M. Khan, and D. McRae: 2000, 'Adaptive grids in air pollution modeling: Towards an operational model'. In: *Millennium NATO/CCMS International Technical Meeting on Air Pollution Modelling and its Applications*. pp. 541–549.

Odman, M., M. Khan, R. Srivastava, and D. McRae: 2002, 'Initial application of the adaptive grid air pollution model'. In: *Air Pollution Modeling and its Application XV: Proceedings of the 25th NATO/CCMS International Technical Meeting on Air Pollution Modeling and Its Application*. pp. 319–328, C. Borrego and G. Schayes, Eds., Kluwer Academic/Plenum Publishers.

Odman, M. and D. McRae: 2003, 'Development and evaluation of modeling techniques for the study of interactions between urban and point source plumes and regional atmospheres in the formation of secondary pollutants'. Technical Report R827028, U.S. Environmental Protection Agency.

Odman, M. and A. Russell: 1991, 'Multiscale modeling of pollutant transport and chemistry'. *Journal of Geophysical Research* **96**, 7363–7370.

Olson, K.: 2006, 'PARAMESH: A Parallel Adaptive Grid Tool'. In: A. Deane, A. Ecer, G. Brenner, D. Emerson, J. McDonough, J. Periaux, N. Satofuka, and D. Tromeur-Dervout (eds.): *Parallel CFD Conference*. Elsevier.

Olson, K. and P. MacNeice: 2005, 'An Overview of the PARAMESH AMR Software and Some of Its Applications'. *Adaptive Mesh Refinement-Theory and Applications, Proceedings of the Chicago Workshop on Adaptive Mesh Refinement Methods* **41**.

Park, R., K. Pickering, D. Allen, G. Stenchikov, and M. Fox-Rabinovitz: 2004, 'Global simulation of tropospheric ozone using the University of Maryland Chemical Transport Model (UMD-CTM): 2. Regional transport and chemistry over the central United States using a stretched grid'. *Journal of Geophysical Research* **109**, D09303.

Pilke, R., W. Cotton, R. Walko, C. Tremback, W. Lyons, L. Graso, M. Nocholls, M. Moran, D. Wesley, T. Lee, and J. Copeland: 1992, 'A Comprehensive Meteorological Modeling System - RAMS.'. *Meteorol. Atmos. Phys.* **49**, 69–91.

SAIC: 2003, 'Operational Multiscale Environment model with Grid Adaptivity (OMEGA)'. *SAIC URL: http://www.saic.com/omega*. Science Applications International Corporation.

Sandu, A. and E. Constantinescu: 2007, 'Multirate explicit Adams methods for time integration of conservation laws'. *Submitted to Journal of Scientific Computing*.

Sandu, A., D. Daescu, G. Carmichael, and T. Chai: 2005, 'Adjoint sensitivity analysis of regional air quality models'. *Journal of Computational Physics* **204**, 222–252.

Srivastava, R., D. McRae, and M. Odman: 2001a, 'Simulation of a reacting pollutant puff using an adaptive grid algorithm'. *Journal of Geophysical Research* **106**(D20), 24,245–24,257.

Srivastava, R., D. McRae, and M. Odman: 2001b, 'Simulation of dispersion of a power plant plume using an adaptive grid algorithm'. *Atmospheric Environment* **35**(28), 4801–4818.

Tomlin, A., M. Berzins, J. Ware, J. Smith, and M. Pilling: 1997, 'On the use of adaptive gridding methods for modelling chemical transport from multi-scale sources'. *Atmospheric Environment* **31**(18), 2945–2959.

Unal, A. and M. Odman: 2003, 'Adaptive Grid Modeling for Predicting the Air Quality Impacts of Biomass Burning'. In: *5th Symposium on Fire and Forest Meteorology*.

van Loon, M.: 1996, 'Numerical Methods in Smog Prediction'. Ph.D. thesis, Proefschrift Universiteit van Utrecht, Utrecht.

Verwer, J., E. Spee, J. Blom, and W. Hundsdorfer: 1999, 'A second order Rosenbrock method applied to photochemical dispersion problems'. *SIAM J. Sci. Comput.* **20**(4), 1456–1480.

Wang, Y., M. McElroy, D. Jacob, and R. Yantosca: 2004, 'A nested grid formulation for chemical transport over Asia: Applications to CO'. *Journal of Geophysical Research* **109**, D22307.